ADVANCED MATERIALS
www.advmat.de

Strongly Correlated Exciton-Magnetization System for Optical Spin Pumping in $CrBr_3$ and CrI_3.

*M. Grzeszczyk, S. Acharya, D. Pashov, Z. Chen, K. Vaklinova, M. van Schilfgaarde, K. Watanabe, T. Taniguchi, K. S. Novoselov, M. I. Katsnelson, and M. Koperski**

Ferromagnetism in van der Waals systems, preserved down to a monolayer limit, attracted attention to a class of materials with general composition CrX_3 (X=I, Br, and Cl), which are treated now as canonical 2D ferromagnets. Their diverse magnetic properties, such as different easy axes or varying and controllable character of in-plane or interlayer ferromagnetic coupling, make them promising candidates for spintronic, photonic, optoelectronic, and other applications. Still, significantly different magneto-optical properties between the three materials have been presenting a challenging puzzle for researchers over the last few years. Herewith, it is demonstrated that despite similar structural and magnetic configurations, the coupling between excitons and magnetization is qualitatively different in $CrBr_3$ and CrI_3 films. Through a combination of the optical spin pumping experiments with the state-of-the-art theory describing bound excitonic states in the presence of magnetization, we concluded that the hole-magnetization coupling has the opposite sign in $CrBr_3$ and CrI_3 and also between the ground and excited exciton state. Consequently, efficient spin pumping capabilities are demonstrated in $CrBr_3$ driven by magnetization via spin-dependent absorption, and the different origins of the magnetic hysteresis in $CrBr_3$ and CrI_3 are unraveled.

1. Introduction

The observation of ferromagnetism in van der Waals crystals down to a monolayer limit[1–6] opened a new avenue for the exploration of the physics and the functionality of 2D magnetic order.[7–20] Ferromagnetic layers host strongly correlated electronic states that give rise to diverse band structures including metallic, semiconducting, or insulating characteristics.[21–23] Among them, the chromium trihalides[24–40] (CrX_3) display unique electronic properties predominantly driven by the Cr *d*-shell electrons that simultaneously contribute to Cr–Cr ferromagnetic coupling, wide band gap, and strongly bound excitonic states. Consequently, the magnetization state of the CrX_3 crystals is intimately related to their magneto-optical properties. Ferromagnetism-induced hysteretic optical signals were observed through photoluminescence[41] (PL), Kerr rotation,[42] or circular dichroism measurements. These results unveiled ferromagnetic coupling between the Cr spins within a monolayer plane with easy axis magnetization oriented out-of-plane for $CrBr_3$ and CrI_3 and in-plane for $CrCl_3$, thickness-dependent interplane ferromagnetic and antiferromagnetic coupling in CrI_3 multilayers as well as light-mediated ferromagnetic response in doped transition metal dichalcogenides.[43–45] Unfortunately, these optical methods have only been used as magnetization probes while the interplay between the magnetic state and the optical excitations remains unexplored.

M. Grzeszczyk, Z. Chen, K. Vaklinova, K. S. Novoselov, M. Koperski
Institute for Functional Intelligent Materials
National University of Singapore
Singapore 117544, Singapore
E-mail: msemaci@nus.edu.sg

S. Acharya, M. I. Katsnelson
Institute for Molecules and Materials
Radboud University
AJ Nijmegen NL-6525, The Netherlands

S. Acharya, M. van Schilfgaarde
National Renewable Energy Laboratory
Golden, CO 80401, USA

The ORCID identification number(s) for the author(s) of this article can be found under https://doi.org/10.1002/adma.202209513.

DOI: 10.1002/adma.202209513

D. Pashov, M. van Schilfgaarde
King's College London
Theory and Simulation of Condensed Matter
The Strand, London WC2R 2LS, UK

K. Watanabe
Research Center for Functional Materials
National Institute for Materials Science
Tsukuba 305-0044, Japan

T. Taniguchi
International Center for Materials Nanoarchitectonics
National Institute for Materials Science
Tsukuba 305-0044, Japan

K. S. Novoselov, M. Koperski
Department of Materials Science and Engineering
National University of Singapore
Singapore 117575, Singapore

The incomplete understanding of the correlated exciton-magnetization states constitutes a bottleneck in further developments of the two-dimensional ferromagnetic structures and devices. An important aspect of such interplay is the ability to optically pump the electronic spins. In $CrBr_3$ and CrI_3 the easy-axis anisotropy enables out-of-plane magnetization direction, which *in principle* can favor particular spin alignments within the photo-excited excitonic population, leading to plausible mechanisms of controlling the spin and/or magnetization properties of the material with light.

Herewith, we demonstrate that the excitonic spin physics is dramatically different between $CrBr_3$ and CrI_3. The light absorption related to resonant photo-creation of excited exciton states is strongly spin-dependent in $CrBr_3$ in the presence of a saturated ferromagnetic state under circularly polarized sub-bandgap excitation. An analogous experiment for CrI_3 demonstrates no significant sensitivity to the polarization state of the excitation photons. Furthermore, the substantial difference between the two ferromagnetic materials is reversed when observing the light emitted from the excitonic ground state – $CrBr_3$ layers emit non-polarized light while CrI_3 layers emit strongly polarized light. Contrasting excitonic spin physics in the presence of ferromagnetic order between CrI_3 and $CrBr_3$ is non-trivial and requires a novel theoretical approach to describing the excitonic states in strongly correlated systems. To that end, we develop an atomically-, orbitally- and spin-resolved higher-order electron-hole ladder vertex corrected quasi-particle self-consistent extension of GW,[46,47] called QSG$\hat{W}$,[48] capturing the Frenkel, charge-transfer and Wannier–Mott characteristics of the ground and excited excitonic states in $CrBr_3$ and CrI_3. The resulting opposite (anti-)ferromagnetic character of the coupling between the hole and the magnetization in $CrBr_3$ and CrI_3 and between ground and excited exciton states within the same material was found to be consistent with the findings of the optical pumping experiments. The varying interactions between excitons and magnetization in the two seemingly similar van der Waals ferromagnets prove the qualitatively different origin of the magnetic hysteresis, open pathways towards perturbing the magnetization via optical methods and imply the existence of the spin glass state in CrI_3 layers due to less localized excitonic states in the presence of magnetic domain structure.

2. Results and Discussion

2.1. Molecular Excitons in $CrBr_3$ and CrI_3

We begin the analysis of the optical response of $CrBr_3$ and CrI_3 at 1.6 K by inspecting the PL and quasi-absorption PL excitation (PLE) spectra of mechanically exfoliated bulk samples. Both materials feature an optical response dominated by broad emission and absorption bands as demonstrated in **Figure 1**a,b. These spectra are characteristic of molecular crystals, where excitons exhibit strong localization in real space down to the ultimate limit of individual atoms or molecules. Therefore, the effective mass approximation is not applicable. The exciton recombination follows the rules of the molecular Franck–Condon model instead. The processes of light absorption/emission involve transitions between electronic levels with simultaneous creation/annihilation of phonons leading to the observation of phonon sidebands in absorption and emission spectra. These many-body processes give rise to long microsecond decay times illustrated in Figure 1c,d. It is worth noting that PL decay for CrI_3 is much faster than for $CrBr_3$ and has a qualitatively different dependence on time *t*. The decay transient for $CrBr_3$ is monoexponential (see Figure 1c), while for CrI_3 it is described by a stretched exponential function with sub-linear index $t^{0.3}$ (see Figure 1d). Such stretched exponential relaxation is known for glasses (Kohlrausch exponent[49]), but in the context of excitonic recombination, it looks quite exotic. We preliminarily attribute the unusual recombination of excitons in CrI_3 to the self-induced spin glass state in ferromagnetic thin films[50] in the presence of irregular magnetic domain structure[51] observed experimentally in CrI_3. Beyond the discussed phonon sideband, the direct transition between the electronic states yields a zero-phonon line (ZPL), which we observe in $CrBr_3$ as a narrow resonance with a linewidth of 400 ± 100 μeV at 1.48 eV.

The spectra consist of numerous broad emission and absorption bands. The emission sidebands are centered at 1.2 eV for CrI_3 and 1.3 eV for $CrBr_3$. It does not follow, however, that the energy scales generating the excitons are similar. On the contrary, the GW calculations[52,53] demonstrate that the bulk single-particle band gap yields 3.8 eV for $CrBr_3$ and 2.4 eV for CrI_3 with the ground exciton binding energy of 2.5 eV for $CrBr_3$ and 1.2 eV for CrI_3. Our calculations of the excitonic wave function in $CrBr_3$ and CrI_3 (Figure 1e,f) indicate that the ground excitonic state exhibits strong Frenkel and charge-transfer characteristics. That signifies that the excitonic excitation occurs virtually within CrX_3 molecule. Multiple valence and conduction bands contribute to the ground excitonic states,[53] which are made mostly of *d*-orbitals of chromium atom: e_g for the conduction band and t_{2g} for the valence band. The minority contribution originates from the *p*-states or the halide atom (Br or I). Therefore, it is tempting to write the excitonic wave function as:

$$\psi_X = \alpha\psi_{Cr,d} + \beta\psi_{Br/I,p} \quad (1)$$

where ψ_X is the Frenkel exciton wave function, $\psi_{Cr,\,d}$ represents the majority contribution from chromium *d*-orbitals and $\psi_{Br/I,\,p}$ represents the minority contribution from halogen *p*-orbitals. $\psi_{Cr,d}$ is a dark exciton as the d-d type of transition between e_g and t_{2g} states is forbidden by the symmetry of the participating states (Laporte rule as seen in Figure 1g). Therefore, CrX_3 materials can be considered fundamentally dark. The observable PL arises due to the brightening of dark excitons. Based on the composition of the excitonic wave function in combination with the comparative analysis of PL and PLE spectra we identify two brightening mechanisms: 1) admixtures of bright *p*-type orbitals of the halide atoms into the excitonic wave function which gives rise to the ZPL[54,55] and 2) recombination/creation of dark $\psi_{Cr,d}$ state through many-body processes with the emission/absorption of phonons. The latter processes give rise to broad emission/absorption bands at the lower/higher energy side of the ZPL as highlighted in Figure 1a. Within the molecular picture according to the Franck-Condon model (Figure 1h), CrX_3 materials are characterized by an extremely small Debye-Waller factor (6.5×10^{-5} for $CrBr_3$) equivalent to

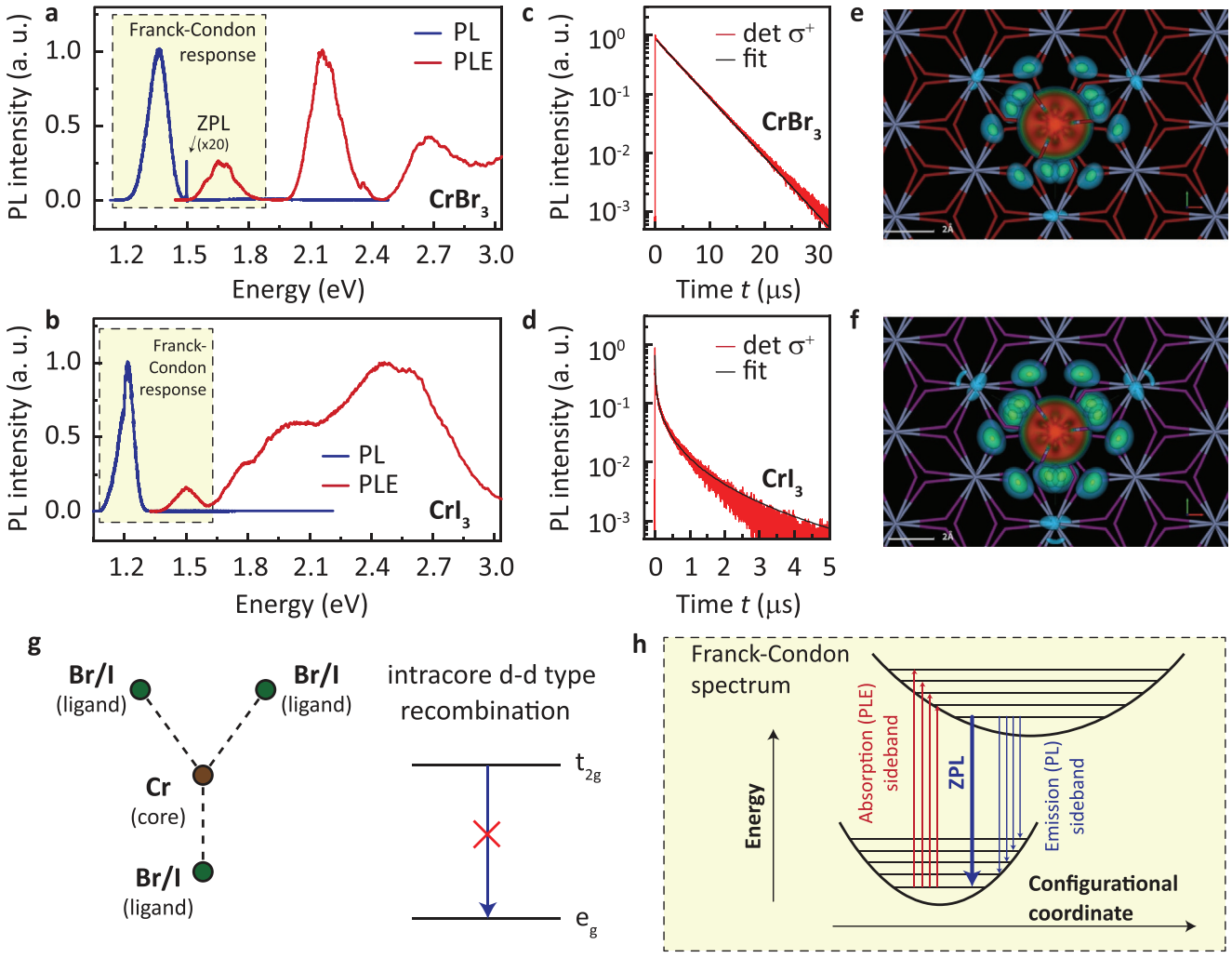

Figure 1. The PL (blue curves) and PL excitation (red curves) spectra were measured at 1.6 K for a) $CrBr_3$ and b) CrI_3 exfoliated bulk films encapsulated in hBN layers. The PL decay times were measured in the same conditions under picosecond laser excitation by spectrally integrating the circularly polarized PL intensity over the entire emission bands for c) $CrBr_3$ and d) CrI_3 . The PL transient for $CrBr_3$ was fitted with a monoexponential decay $I(t) = A\exp -t/\tau$ with $\tau = 4.3 \pm 0.4$ µs. The PL transient for CrI_3 was fitted with a stretched exponential decay $I(t) = A\exp(-t/\tau)^n$ with $\tau = 6.9 \pm 0.6$ ns, $n = 0.30 \pm 0.02$. The ground state excitonic wave functions were calculated in the framework of QSGŴtheory for e) $CrBr_3$ and f) CrI_3. The probability density, from low to high, is represented by isosurfaces in colors blue to red (for details see Appendix, Supporting Information). In a simple picture, the excitonic excitation occurs mostly within the CrX_3 molecule with the dominant recombination channel related to the transition between t_{2g} and e_g states of the Cr *d*-orbitals as schematically illustrated in g). Consequently, the low energy optical response of CrX_3 materials follows a molecular Franck-Condon model h), where the transition between the electronic states is accompanied by the emission and absorption of optical phonons.

a Huang–Rhys factor of 9.6.[56] These figures of merit indicate that the dominant radiative recombination channel for the ground excitonic state in $CrBr_3$ involves phonon-assisted recombination of dark $\psi_{Cr,\,d}$ state.

2.2. Optical Spin Pumping in $CrBr_3$ and CrI_3.

Inspection of the PL intensity associated with the phonon sidebands in $CrBr_3$ and CrI_3 resolved by circular polarization in a magnetic field demonstrates a hysteresis indicative of the intrinsic ferromagnetic order. We introduce circularly polarized excitation in a resonant sub-bandgap regime based on the PLE data with the laser energy tuned to 1.6 eV for $CrBr_3$ and 2.4 eV for CrI_3. Monitoring the PL intensity in the four possible co- and cross-polarized excitation/detection scenarios in both directions of the varying magnetic field unveils striking differences between $CrBr_3$ and CrI_3 as seen in **Figure 2**a–d. The $CrBr_3$ exhibit a sharp hysteresis with a coercive field of 235 ± 10 mT characteristic of in-plane and interlayer ferromagnetic coupling. The hysteresis observed for CrI_3 is more complex, displaying multiple magnetization steps and higher field hysteresis loops up to about 2 T. These additional features have been attributed to the coexistence of antiferromagnetic and ferromagnetic interlayer coupling, which were found to be dependent on stacking types and/or rotational alignment.[57–61]

Beyond the characteristics of the magnetic order, further differences arise from the spin properties of the photo-created excitons. In the saturated bulk ferromagnetic state, the light

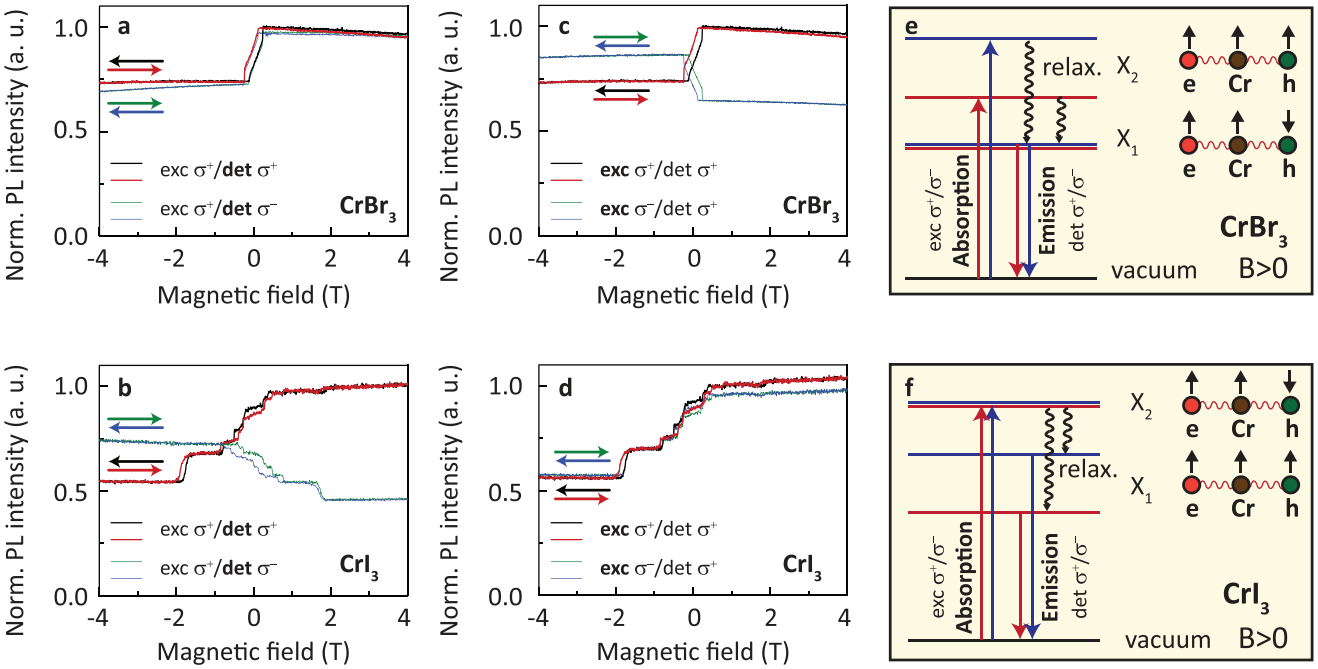

Figure 2. The magneto-photolPL) intensity of the phonon sideband was measured under the circularly polarized laser excitation ($\sigma^{+/-}$) and the emitted light was resolved by circular polarization ($\sigma^{+/-}$). The magnetic field was applied out-of-plane of the CrX_3 layers and the hysteretic features were observed by sweeping the magnetic field in both directions. In such conditions, the spin properties of the ground exciton state were studied by monitoring the magneto-PL intensity under fixed excitation (σ^{+}) and varied detection (σ^{+} or σ^{-}) for a) $CrBr_3$ and b) CrI_3. The spin properties of the excited exciton state were studied by monitoring the magneto-PL intensity under varied excitation (σ^{+} or σ^{-}) and fixed detection (σ^{+}) for c) $CrBr_3$ and d) CrI_3 . The observed differences in the polarization degree of emitted or absorbed light in both materials are interpreted in terms of the excitonic spin splitting due to the e-Cr and h-Cr exchange coupling for the ground and the excited exciton states as pictorially represented for e) $CrBr_3$ and f) CrI_3.

emitted by $CrBr_3$ exhibits negligible circular polarization degree (Figure 2a). That signifies that an equal number of σ^{+} and σ^{-} active excitons occupy the ground exciton level independently of the magnetization state. Due to the low temperature of the sample (1.6 K), an equal population entails energetic degeneracy of the excitons active in the opposite circular polarizations. The absence of the coupling between the excitonic spin and the magnetization is unlikely due to the observation of the hysteresis. Therefore, the degeneracy of the excitonic state must originate from the compensation of the exchange coupling between the charge carriers and the magnetic moment of the Cr atom contributing to the magnetization, e.g., an electron is coupled ferromagnetically with the magnetization and the hole is coupled antiferromagnetically with the magnetization through interaction with comparable strength (exchange constant). Such interpretation is also consistent with the vanishing g-factor of the ZPL as demonstrated in Appendix in Figure S5 (Supporting Information). On the contrary, CrI_3 films exhibit a significant (up to 37%) polarization degree of the emitted light in the saturated state of the magnetization as seen in Figure 2b. In such a case, the large polarization degree, despite the plausible spin-flip events mediated through optical phonons, implies an energy splitting of the ground excitonic state. For the magnetization-induced exciton splitting to occur, the electron and hole interaction with the magnetic moment of the chromium atom needs to be of the same character (e.g., both ferromagnetic) or they need to differ in strength so that one dominates over another.

The differences in the excitonic spin physics between $CrBr_3$ and CrI_3 are not limited to the polarization properties of the emitted light. For a fixed circular polarization of detected light (σ^{+} in Figure 2c), inspecting the PL intensity from $CrBr_3$ layers under circularly polarized excitation in co- and cross-polarized configurations reveals a polarization degree of the emitted light up to 21%. This observation indicates that the absorption strength related to the resonant creation of an excited exciton state in $CrBr_3$ is spin-dependent. An analogous experiment in CrI_3 demonstrates negligible polarization degree of the emitted light implying that the absorption strength is not spin-dependent. The general view, which arises from the polarization-resolved magneto-PL experiments for $CrBr_3$ and CrI_3, is that the coupling between photo-excited charge carriers is material-dependent and varies between the ground and the excited excitonic states. The ground exciton state in $CrBr_3$ is coupled to magnetization qualitatively akin to the excited exciton state in CrI_3 and vice versa. Additional measurements performed on a single layer of $CrBr_3$ revealed the excitonic spin pumping is universal across various thicknesses, as summarized in Appendix in Section S4 (Supporting Information). We interpret this observation by considering the excitonic splitting due to electron-Cr and hole-Cr exchange interactions as pictorially demonstrated in Figure 2e,f. We now proceed to the discussion about the origin of the distinct coupling between the excitonic spin with the magnetization in terms of the quasi-particle self-consistent QSG$\hat{W}$ theory.

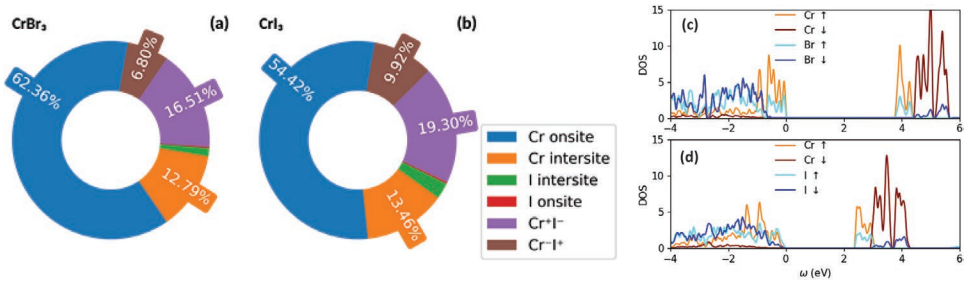

Figure 3. The calculations of the excitonic ground state via QSG$\hat{W}$ reveal the atomic contribution of electrons and holes separately. Their contributions are presented in form of a pie chart for a) $CrBr_3$ and b) CrI_3. They include Frenkel intra-Cr and intra-halide states and charge-transfer Cr-halide and Cr-Cr (intermolecular) states. The atom- and spin-resolved density of states is shown for bulk c) $CrBr_3$ and d) CrI_3.

2.3. Atomically-, Orbitally-, and Spin-Resolved Excitonic Band Structure in $CrBr_3$ and CrI_3.

We firstly focus on the excitonic ground state in $CrBr_3$ and CrI_3. In many excitonic systems with charge carriers describable within the effective mass approximation, the atomic localization of one of the carriers is assumed based on its physical properties (e.g., larger effective mass) to calculate the range of the exciton wave function. In $CrBr_3$ and CrI_3, the ground state excitons are localized to a degree that they are not sensitive to the periodicity of the lattice. As such, the contributions to the excitonic ground state wave functions originate from the entire Brillouin zone and multiple sub-bands rather than from the band edges at the specific points of the reciprocal lattice.[53] As such, there is no clear physical distinction between the electron and hole states that would favor the localization of any type of carrier. Therefore, we calculated the atomically-resolved ground excitonic wave functions for $CrBr_3$ and CrI_3 in a general case as demonstrated in **Figure 3**a,b. We found that in both materials there are two major contributions: the Frenkel-type excitation when both the electron and the hole are located on the same Cr atom and the charge-transfer-type excitation when the electron and the hole occupy two different atoms. The latter contribution includes cases when the electron and the hole are distributed between the Cr atom and the halide atom or between two Cr atoms (within two neighboring molecules). A very minor contribution originates also from Frenkel-type intra-halide states. Although $CrBr_3$ and CrI_3 exhibit qualitatively similar compositions of the excitonic ground state, $CrBr_3$ is characterized by the larger Frenkel component implying stronger localization of the excitonic wave function, as expected from larger excitonic binding energy. The detailed differences between the excitonic ground state for $CrBr_3$ and CrI_3 bulk films, including an orbital resolution at individual atom sites, are summarized in Appendix in Figure S11 (Supporting Information).

Given the intra- and inter-atomic localization of the ground exciton state, the orbitally-resolved density of states (DOS) directly (Figure 3c,d) explains the varying character of the excitonic coupling with magnetization as demonstrated experimentally. Firstly, we note that in the energy range of the conduction bands in $CrBr_3$ and CrI_3 the Cr *d*-orbitals constitute the dominant contribution to the DOS. Therefore, independently of the excitonic localization, the e-Cr interaction will have a ferromagnetic character. The qualitative difference arises from the composition of the valence band. In $CrBr_3$, the valence band is dominantly formed of the Cr *d*-orbitals up to about 1 eV away from the valence band edge. At that energy, the composition abruptly changes, so that the higher energy bands consist almost exclusively of Br *p*-orbitals characterized by the opposite spin with respect to the Cr atom. Consequently, the highly localized Frenkel character of the ground state exciton in $CrBr_3$ will impose summation over multiple valence bands, leading to the antiferromagnetic character of the h-Cr interaction. In CrI_3, the Cr and I contribution to the valence band is comparable up to about 1.5 eV away from the valence band edge. Also, the ground state exciton is less localized in CrI_3 than in $CrBr_3$, so the sub-bands closer to the band edge will contribute to its wave function. Consequently, the h-Cr interaction in the ground exciton state will likely be small due to the competition between the ferromagnetic coupling from Cr *d*-orbitals and antiferromagnetic coupling from I *p*-orbitals, leaning closer towards the ferromagnetic character.

The excited excitonic states partially recover the Wannier–Mott character, so that the exciton derives more from the states near the valence band maximum and conduction band minimum than the ground state case. Our calculations demonstrate that the valence band edge in $CrBr_3$ is mainly comprised of Cr *d*-orbitals implying ferromagnetic h-Cr coupling in the excited excitonic state while the valence band edge in CrI_3 consists predominantly of the halide *p*-orbitals, implying antiferromagnetic h-Cr coupling. Overall, the character of the interactions between the carriers and magnetization deduced from the optical pumping experiments in combination with QSG$\hat{W}$ description of the excitonic states is summarized in **Table 1**. We note that previous theoretical works[62,63] captured the flip in the sign of the coupling between electrons/holes and the magnetic moment on Cr, between $CrBr_3$ and CrI_3 and between the ground and excited states. However, our combined

Table 1. The summary of the character of the coupling between electrons/holes and the magnetic moment of the Cr atom for $CrBr_3$ and CrI_3 in the ground and excited state. FM stands for ferromagnetic, AFM stands for antiferromagnetic.

	Ground excitonic state		Excited excitonic state	
	Cr-electron	Cr-hole	Cr-electron	Cr-hole
$CrBr_3$	FM	AFM	FM	FM
CrI_3	FM	FM (small exchange constant)	FM	AFM

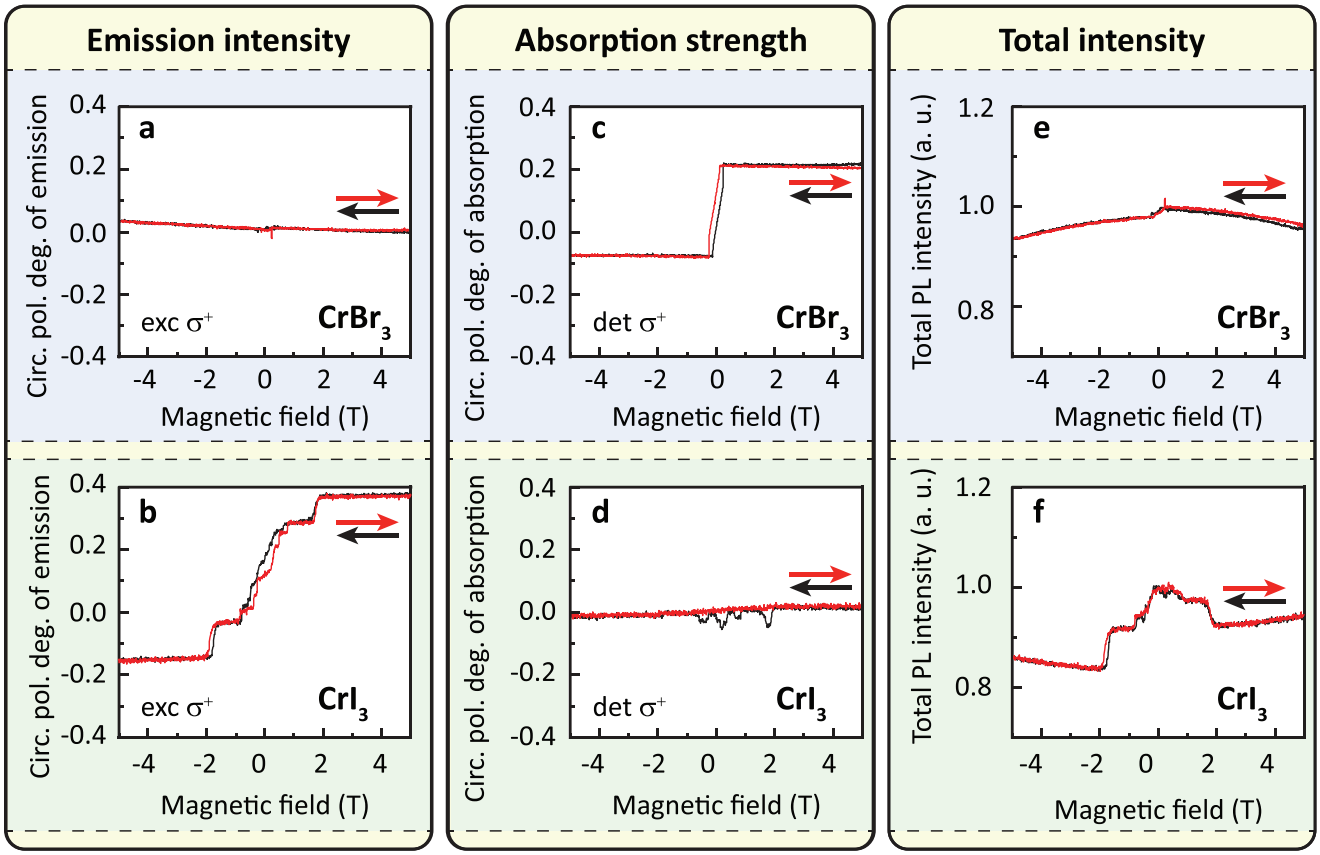

Figure 4. The origin of the hysteresis in the magneto-PL experiments. The polarization degree of the emitted light, defined as $(I_{\sigma^+} - I_{\sigma^-})/(I_{\sigma^+} + I_{\sigma^-})$ under fixed excitation was monitored as a function of a magnetic field in both sweeping directions for a) $CrBr_3$ and b) CrI_3 . Only in CrI_3 the hysteresis is observable in such experiments. Similarly, the polarisation degree of absorbed light for σ^+ fixed detection was monitored as a function of a magnetic field in both sweeping directions for c) $CrBr_3$ and d) CrI_3 . In such a configuration, the hysteresis appears only in $CrBr_3$. When monitoring the total PL intensity, defined as $I_{\text{total}} = \sum_{i=+,-} \sum_{j=+,-} I_{\text{exc } \sigma^i, \text{det } \sigma^j}$ for e) $CrBr_3$ and f) CrI_3 , the higher field hysteretic features appear in CrI_3 that are attributed to the breaking of interlayer antiferromagnetic coupling.

experimental and theoretical approaches come to a somewhat different conclusion related to the sign of the e-Cr coupling. This can be traced to the effect of quasiparticle self-consistency, which modifies the charge density[64] relative to the LDA (or LDA+U). Self-consistency gives rise to an important change in the lowest unoccupied eigenstates, causing the lowest conduction bands to take predominately Cr character (see DOS in Figure 3c,d). The electron component of the exciton is, in the QSGW case, always aligned with the majority spin. The QSGW result is not biased by the LDA starting point as is the case with single-shot GW calculations.

Our findings have several consequences for the investigation of magnetism through optical methods. Firstly, the hysteretic signals observed in the PL experiments have a different origin in $CrBr_3$ and CrI_3 as illustrated in **Figure 4**a–f. In $CrBr_3$ the hysteresis is witnessed exclusively through the modulation of the absorption strength. In CrI_3 the hysteresis appears via the modulation of the polarization degree of the emitted light through a thermally populated ground state. However, the higher field loops (e.g., those around 2 T) are seen in the total emission intensity (i.e., intensity summed over all four possible co- and cross-polarized configurations). That indicates the presence of a non-radiative process, which is mostly responsible for probing the antiferromagnetic interlayer coupling. These mechanisms are summarized in **Table 2**.

3. Conclusion

In summary, we have demonstrated that the type of ferromagnetic coupling between the excitonic spin and magnetization determines the spin physics in CrX_3 materials. The excitonic spins can be pumped in $CrBr_3$ through a spin-dependent absorption process due to e-Cr and h-Cr ferromagnetic coupling

Table 2. The mechanism of the observation of the magnetization-related hysteretic features in magneto-PL experiments based on the optical pumping experiments and the composition of the excitonic states based on QSGŴ theory.

	Mechanism of hysteresis observation		
	Exciton population on emitting state	Modulation of absorption strength	Spin-dependent non-radiative process
$CrBr_3$	✗	✓	✗
CrI_3	✓	✗	✓

in the exited sub-band-gap state. Such process does not occur in CrI_3, as the h-Cr becomes antiferromagnetic in the excited exciton state as a result of the recovered Wannier–Mott character. The unique interplay between excitons and magnetization furthers the understanding of strongly correlated systems and constitutes a foundation for spintronics applications in van der Waals systems controlled by light.

Supporting Information

Supporting Information is available from the Wiley Online Library or from the author.

Acknowledgements

This project was supported by the Ministry of Education (Singapore) through the Research Centre of Excellence program (grant EDUN C-33-18-279-V12, I-FIM). This material was based upon work supported by the Air ForceEuropean office of Aerospace Research and Development Office of Scientific Research and the Office of Naval Research Global under award number FA8655-21-1-7026. The work of S.A. and M.I.K. was supported by the European Research Council via Synergy Grant No. 854843-FASTCORR. M.v.S., S.A., D.P. were supported at the National Renewable Energy Laboratory, Operated by the Alliance for Sustainable Energy, for the US Department of Energy, Basic Energy Sciences, Division of Computational Chemical Sciences under Contract No. DE-AC36-08GO28308. This research used resources of the National Energy Research Scientific Computing Center (NERSC), award BES-ERCAP0021783, under DOE Contract No. DE-AC02-05CH11231. S.A. and M.I.K. acknowledge PRACE for awarding us access to Irene-Rome hosted by TGCC, France. The work was supported by the National Science Centre, Poland (Grant No. 2020/37/B/ST3/02311).

Conflict of Interest

The authors declare no conflict of interest.

Data Availability Statement

The data that support the findings of this study are available from the corresponding author upon reasonable request.

Keywords

2D ferromagnets, excitons, optical spin pumping, origin of hysteresis

Received: October 16, 2022
Revised: January 13, 2023
Published online: March 15, 2023

[1] B. Huang, G. Clark, E. Navarro-Moratalla, D. R. Klein, R. Cheng, K. L. Seyler, D. Zhong, E. Schmidgall, M. A. McGuire, D. H. Cobden, W. Yao, D. Xiao, P. Jarillo-Herrero, X. Xu, *Nature* **2017**, *546*, 270.
[2] C. Gong, L. Li, Z. Li, H. Ji, A. Stern, Y. Xia, T. Cao, W. Bao, C. Wang, Y. Wang, Z. Q. Qiu, R. J. Cava, S. G. Louie, J. Xia, X. Zhang, *Nature* **2017**, *546*, 265.
[3] S. Liu, X. Yuan, Y. Zou, Y. Sheng, C. Huang, E. Zhang, J. Ling, Y. Liu, W. Wang, C. Zhang, J. Zou, K. Wang, F. Xiu, *npj 2D Mater. Appl.* **2017**, *1*, 1.
[4] M. Bonilla, S. Kolekar, Y. Ma, H. C. Diaz, V. Kalappattil, R. Das, T. Eggers, H. R. Gutierrez, M.-H. Phan, M. Batzill, *Nat. Nanotechnol.* **2018**, *13*, 289.
[5] D. J. O'Hara, T. Zhu, A. H. Trout, A. S. Ahmed, Y. K. Luo, C. H. Lee, M. R. Brenner, S. Rajan, J. A. Gupta, D. W. McComb, R. K. Kawakami, *Nano Lett.* **2018**, *18*, 3125.
[6] Z. Fei, B. Huang, P. Malinowski, W. Wang, T. Song, J. Sanchez, W. Yao, D. Xiao, X. Zhu, A. F. May, W. Wu, D. H. Cobden, J.-H. Chu, X. Xu, *Nat. Mater.* **2018**, *17*, 778.
[7] M. Weisheit, S. FÃhler, A. Marty, Y. Souche, C. Poinsignon, D. Givord, *Science* **2007**, *315*, 349.
[8] T. Maruyama, Y. Shiota, T. Nozaki, K. Ohta, N. Toda, M. Mizuguchi, A. Tulapurkar, T. Shinjo, M. Shiraishi, S. Mizukami, Y. Ando, Y. Suzuk, *Nat. Nanotechnol.* **2009**, *4*, 158.
[9] W.-G. Wang, M. Li, S. Hageman, C. Chien, *Nat. Mater.* **2012**, *11*, 64.
[10] F. Matsukura, Y. Tokura, H. Ohno, *Nat. Nanotechnol.* **2015**, *10*, 209.
[11] D. Zhong, K. L. Seyler, X. Linpeng, R. Cheng, N. Sivadas, B. Huang, E. Schmidgall, T. Taniguchi, K. Watanabe, M. A. McGuire, W. Yao, D. Xiao, K.-M. C. Fu, X. Xu, *Sci. Adv.* **2017**, *3*, e1603113.
[12] Y. Deng, Y. Yu, Y. Song, J. Zhang, N. Z. Wang, Z. Sun, Y. Yi, Y. Z. Wu, S. Wu, J. Zhu, J. Wang, X. H. Chen, Y. Zhang, *Nature* **2018**, *563*, 94.
[13] B. Huang, G. Clark, D. R. Klein, D. MacNeill, E. Navarro-Moratalla, K. L. Seyler, N. Wilson, M. A. McGuire, D. H. Cobden, D. Xiao, W. Yao, P. Jarillo-Herrero, X. Xu, *Nat. Nanotechnol.* **2018**, *13*, 544.
[14] S. Jiang, L. Li, Z. Wang, K. F. Mak, J. Shan, *Nat. Nanotechnol.* **2018**, *13*, 549.
[15] Z. Wang, D. Sapkota, T. Taniguchi, K. Watanabe, D. Mandrus, A. F. Morpurgo, *Nano Lett.* **2018**, *18*, 4303.
[16] T. Song, X. Cai, M. W.-Y. Tu, X. Zhang, B. Huang, N. P. Wilson, K. L. Seyler, L. Zhu, T. Taniguchi, K. Watanabe, M. A. Mcguire, D. H. Cobden, D. Xiao, W. Yao, X. Xu, *Science* **2018**, *360*, 1214.
[17] S. Jiang, J. Shan, K. F. Mak, *Nat. Mater.* **2018**, *17*, 406.
[18] K. F. Mak, J. Shan, D. C. Ralph, *Nat. Rev. Phys.* **2019**, *1*, 646.
[19] S. Jiang, L. Li, Z. Wang, J. Shan, K. F. Mak, *Nat. Electron.* **2019**, *2*, 159.
[20] T. Song, M. W.-Y. Tu, C. Carnahan, X. Cai, T. Taniguchi, K. Watanabe, M. A. McGuire, D. H. Cobden, D. Xiao, W. Yao, X. Xu, *Nano Lett.* **2019**, *19*, 915.
[21] K. S. Burch, D. Mandrus, J.-G. Park, *Nature* **2018**, *563*, 47.
[22] M. Gibertini, M. Koperski, A. F. Morpurgo, K. S. Novoselov, *Nat. Nanotechnol.* **2019**, *14*, 408.
[23] Q. H. Wang, A. Bedoya-Pinto, M. Blei, A. H. Dismukes, A. Hamo, S. Jenkins, M. Koperski, Y. Liu, Q.-C. Sun, E. J. Telford, H. H. Kim, M. Augustin, U. Vool, J.-X. Yin, L. H. Li, A. Falin, C. R. Dean, F. Casanova, R. F. L. Evans, M. Chshiev, A. Mishchenko, C. Petrovic, R. He, L. Zhao, A. W. Tsen, B. D. Gerardot, M. Brotons-Gisbert, Z. Guguchia, X. Roy, S. Tongay, et al., *ACS Nano* **2022**, *16*, 6960.
[24] J. Dillon, in *Proceedings of the Seventh Conference on Magnetism and Magnetic Materials*, Springer, Berlin **1962**, pp. 1191–1192.
[25] J. Dillon Jr., J. Remeika, *J. Appl. Phys.* **1963**, *34*, 637.
[26] J. Dillon Jr., C. Olson, *J. Appl. Phys.* **1965**, *36*, 1259.
[27] P. Grant, G. Street, in *Bulletin of the American Physical Society, Amer. Inst. Physics* **1968**, *13*, 415.
[28] I. Pollini, G. Spinolo, *Phys. Status Solidi B* **1970**, *41*, 691.
[29] V. M. Bermudez, D. S. McClure, *J. Phys. Chem. Solids* **1979**, *40*, 129.
[30] L. Nosenzo, G. Samoggia, I. Pollini, *Phys. Rev. B* **1984**, *29*, 3607.
[31] H. Wang, V. Eyert, U. Schwingenschlögl, *J. Phys.: Condens. Matter* **2011**, *23*, 116003.
[32] J. L. Lado, J. Fernández-Rossier, *2D Mater.* **2017**, *4*, 035002.
[33] M. A. McGuire, *Crystals* **2017**, *7*, 121.
[34] M. A. McGuire, G. Clark, K. Santosh, W. M. Chance, G. E. Jellison Jr., V. R. Cooper, X. Xu, B. C. Sales, *Phys. Rev. Mater.* **2017**, *1*, 014001.

[35] H. H. Kim, B. Yang, T. Patel, F. Sfigakis, C. Li, S. Tian, H. Lei, A. W. Tsen, *Nano Lett.* **2018**, *18*, 4885.
[36] Z. Wang, I. Gutiérrez-Lezama, N. Ubrig, M. Kroner, M. Gibertini, T. Taniguchi, K. Watanabe, A. Imamoğlu, E. Giannini, A. F. Morpurgo, *Nat. Commun.* **2018**, *9*, 1.
[37] D. Ghazaryan, M. T. Greenaway, Z. Wang, V. H. Guarochico-Moreira, I. J. Vera-Marun, J. Yin, Y. Liao, S. V. Morozov, O. Kristanovski, A. I. Lichtenstein, M. I. Katsnelson, F. Withers, A. Mishchenko, L. Eaves, A. K. Geim, K. S. Novoselov, A. Misra, *Nat. Electron.* **2018**, *1*, 344.
[38] D. R. Klein, D. MacNeill, J. L. Lado, D. Soriano, E. Navarro-Moratalla, K. Watanabe, T. Taniguchi, S. Manni, P. Canfield, J. Fernández-Rossier, P. Jarillo-Herrero, *Science* **2018**, *360*, 1218.
[39] L. Thiel, Z. Wang, M. A. Tschudin, D. Rohner, I. Gutiérrez-Lezama, N. Ubrig, M. Gibertini, E. Giannini, A. F. Morpurgo, P. Maletinsky, *Science* **2019**, *364*, 973.
[40] X. Cai, T. Song, N. P. Wilson, G. Clark, M. He, X. Zhang, T. Taniguchi, K. Watanabe, W. Yao, D. Xiao, M. A. McGuire, D. H. Cobden, X. Xu, *Nano Lett.* **2019**, *19*, 3993.
[41] K. L. Seyler, D. Zhong, D. R. Klein, S. Gao, X. Zhang, B. Huang, E. Navarro-Moratalla, L. Yang, D. H. Cobden, M. A. McGuire, W. Yao, D. Xiao, P. Jarillo-Herrero, X. Xu, *Nat. Phys.* **2018**, *14*, 277.
[42] N. Sivadas, S. Okamoto, D. Xiao, *Phys. Rev. Lett.* **2016**, *117*, 267203.
[43] V. Ortiz Jimenez, Y. T. H. Pham, M. Liu, F. Zhang, Z. Yu, V. Kalappattil, B. Muchharla, T. Eggers, D. L. Duong, M. Terrones, M.-H. Phan, *Adv. Electron. Mater.* **2021**, *7*, 2100030.
[44] K. Nisi, J. Kiemle, L. Powalla, A. Scavuzzo, T. D. Nguyen, T. Taniguchi, K. Watanabe, D. L. Duong, M. Burghard, A. W. Holleitner, C. Kastl, *Adv. Opt. Mater.* **2022**, *10*, 2102711.
[45] H. Liu, M. T. Trinh, E. M. Clements, D. Sapkota, L. Li, Z. Romestan, S. Bhat, V. Mapara, A. Barua, S. L. Carrera, M.-H. Phan, D. Arena, H. Srikanth, D. Mandrus, A. H. Romero, D. Karaiskaj, *Phys. Rev. B* **2022**, *106*, 035103.
[46] M. van Schilfgaarde, T. Kotani, S. Faleev, *Phys. Rev. Lett.* **2006**, *96*, 226402.
[47] D. Pashov, S. Acharya, W. R. Lambrecht, J. Jackson, K. D. Belashchenko, A. Chantis, F. Jamet, M. van Schilfgaarde, *Comput. Phys. Commun.* **2020**, *249*, 107065.
[48] B. Cunningham, M. Grüning, P. Azarhoosh, D. Pashov, M. Van Schilfgaarde, *Phys. Rev. Mater.* **2018**, *2*, 034603.
[49] J. Rault, *Eur. Phys. J. E* **2012**, *35*, 1.
[50] A. Principi, M. I. Katsnelson, *Phys. Rev. B* **2016**, *93*, 054410.
[51] B. Niu, T. Su, B. A. Francisco, S. Ghosh, F. Kargar, X. Huang, M. Lohmann, J. Li, Y. Xu, T. Taniguchi, K. Watanabe, D. Wu, A. Balandin, J. Shi, Y.-T. Cui, *Nano Lett.* **2019**, *20*, 553.
[52] S. Acharya, D. Pashov, B. Cunningham, A. N. Rudenko, M. Rösner, M. Grüning, M. van Schilfgaarde, M. I. Katsnelson, *Phys. Rev. B* **2021**, *104*, 155109.
[53] S. Acharya, D. Pashov, A. N. Rudenko, M. Rösner, M. v. Schilfgaarde, M. I. Katsnelson, *npj 2D Mater. Appl.* **2022**, *6*, 1.
[54] T. Zhang, M. Grzeszczyk, J. Li, W. Yu, H. Xu, P. He, L. Yang, Z. Qiu, H. Lin, H. Yang, J. Zeng, T. Sun, Z. Li, J. Wu, M. Lin, K. P. Loh, C. Su, K. S. Novoselov, A. Carvalho, M. Koperski, J. Lu, *J. Am. Chem. Soc.* **2022**, *144*, 5295.
[55] In our experiments we observe the narrow excitonic resonance only for thick $CrBr_3$ samples that have been well preserved from degradation processes,[54] as can be seen from the structural characterization of studied flakes presented in Appendix Section S2 (Supporting Information). Theoretically, the intensity of this line should be stronger for CrI_3 due to enhanced admixtures of the *p*-states. However, the energy of CrI_3 emission is located at the edge of sensitivity curves for Si CCD detectors and InGaAs detectors are characterized by significantly larger thermal noise, effectively preventing the observation of weak narrow resonances located on a slope of significantly stronger phonon sideband.
[56] The Debye–Waller factor constitutes the ratio of the ZPL intensity with respect to the total emission intensity (ZPL with phonon sideband). The Huang–Rhys factor was calculated from a phenomenological model that yields $S = -\ln(w)$.
[57] N. Sivadas, S. Okamoto, X. Xu, C. J. Fennie, D. Xiao, *Nano Lett.* **2018**, *18*, 7658.
[58] S. W. Jang, M. Y. Jeong, H. Yoon, S. Ryee, M. J. Han, *Phys. Rev. Mater.* **2019**, *3*, 031001.
[59] P. Jiang, C. Wang, D. Chen, Z. Zhong, Z. Yuan, Z.-Y. Lu, W. Ji, *Phys. Rev. B* **2019**, *99*, 144401.
[60] D. Soriano, C. Cardoso, J. Fernández-Rossier, *Solid State Commun.* **2019**, *299*, 113662.
[61] Y. Xu, A. Ray, Y.-T. Shao, S. Jiang, K. Lee, D. Weber, J. E. Goldberger, K. Watanabe, T. Taniguchi, D. A. Muller, K. F. Mak, J. Shan, *Nat. Nanotechnol.* **2022**, *17*, 143.
[62] M. Wu, Z. Li, T. Cao, S. G. Louie, *Nat. Commun.* **2019**, *10*, 1.
[63] M. Wu, Z. Li, S. G. Louie, *Phys. Rev. Mater.* **2022**, *6*, 014008.
[64] S. Acharya, D. Pashov, A. N. Rudenko, M. Rösner, M. van Schilfgaarde, M. I. Katsnelson, *npj Comput. Mater.* **2021**, *7*, 1.